Composite Structures 286 (2022) 115305

Contents lists available at ScienceDirect

Composite Structures

journal homepage: www.elsevier.com/locate/compstruct

Structure health monitoring of a composite wing based on flight load and strain data using deep learning method

Minxiao Lin [a], Shijun Guo [a,*], Shun He [a,b], Wenhao Li [a,c], Daqing Yang [d]

[a] Centre for Aeronautics, School of Aerospace, Transport and Manufacturing, Cranfield University, Cranfield MK43 0AL, UK
[b] School of Aeronautics, Northwestern Polytechnical University, Xi'an 710072, PR China.
[c] Advanced Manufacturing Center, Ningbo Institute of Technology, Beihang University, Ningbo 315832, PR China
[d] Department of Aeronautics, Imperial College London, London SW7 2BX, UK

ARTICLE INFO

Keywords:
Composite wing
Structural health monitoring
Convolutional neural network
Digital twin

ABSTRACT

An investigation was made into a method for Structural Health Monitoring (SHM) of a composite wing using Convolutional Neural Network (CNN) model. In this method, various aerodynamic loads of an aircraft during flight and corresponding strain data were used for CNN model training. The proposed method was demonstrated by numerical simulation using vortex lattice method for aerodynamic loads of an A350-type aircraft in over a thousand flight conditions and a Finite Element (FE) model as a digital twin of the full-scale composite wing. To represent the measurement of 324 sensors mounted in the 18 skin-rib joints of the inboard wing, strain data from the 18 × 18 elements of the FE model in the sensor locations were calculated corresponding to the flight loadings. The strain data from the original structure FE model were employed to train a CNN model that was classified as healthy samples. Damaged elements were then introduced in random locations to produce data samples corresponding to the same set of flight loads for the CNN model training. In the subsequent damage detection process using the trained CNN model, confusion matrix, uncertainty and sensitivity analysis were evaluated. The study results show that robust damage detection results can be obtained with 99% accuracy without noise and 97% accuracy with 2% Gaussian noise. In the damage localization process, threshold value was set at 1.5, 2 or 2.5, and 83% overall accuracy was achieved using the CNN model when the threshold value was 1.5. The study demonstrated that the proposed method is efficient, accurate and robust.

1. Introduction

Composite materials especially laminated carbon fibre reinforced plastics have superior mechanical performance and large weight saving potential for airframe structures due to their significantly higher specific stiffness and strength properties than traditional metallic materials. This has led to dramatic increase of composite materials usage in large civil airplanes such as A350 and the B-787 in the last decade [1–4]. However, laminated composite materials are prone to various inconspicuous damages that may lead to failure in different modes, such as fiber breakage, matrix crack and delamination [5–8]. This feature raises a major concern on composite structure integrity that reduces significantly the safety margin in the design and weight saving in practice. In addition, non-reinforced composite laminate through thickness is prone to transverse loading. This raises a concern on load transfer capability of bonded structure joint and mechanical failure. Therefore, the conventional joint connection using rivets and bolts is adapted in the state-of-the-art bonded composite airframe joint to ensure its structural integrity.

In order to fully explore the potential of airframe structures using composite materials, early detection of damages or defects is important. Unlike the metallic skin however, an impact damage in laminated composite skin is normally barely visible hence difficult to detect by observation or image processing. A Structural Health Monitoring (SHM) system in particular an onboard one based on sensing technology provides an effective means for damage detection of composite airframe. The state-of-the-art SHM systems utilize various measurement techniques including strain, ultrasonic guided waves, vibration signal or electromechanical impedance to form a sensor network installed on the structures alongside with data processing [9,10]. The strain and vibration signal measurement as a mature technique has been employed to detect structural damage using modal test data in 1990's [11,12]. This

* Corresponding author.
E-mail address: s.guo@cranfield.ac.uk (S. Guo).

https://doi.org/10.1016/j.compstruct.2022.115305
Received 30 June 2021; Received in revised form 24 December 2021; Accepted 23 January 2022
Available online 29 January 2022
0263-8223/© 2022 The Authors. Published by Elsevier Ltd. This is an open access article under the CC BY-NC-ND license (http://creativecommons.org/licenses/by-nc-nd/4.0/).

approach relies on the fact that a local stiffness degradation due to structural damage leads to a measurable strain redistribution in the sensing region. However, it is unpractical to embed strain gauges, optical fibres or accelerometers in the laminate or install on the structure surface. A large number of strain-based SHM studies for aircraft structures have been carried out in literature, but the majority demonstrated the technology by taking panel or beam test samples under simple loading scenarios.

To find a practical solution, Guo and Li [2,13] developed a composite fastener as an alternative to the conventional metallic rivet for composite structure joint reinforcement. The composite fastener has been further developed into a novel Smart Composite Fastener (SCF) with embedded sensor and micro transmitter. Taking a composite wing as example, at least a few percent of the tens of thousands metallic rivets distributed in the structure joints could be replaced by the SCF to form a sensing network. Since those joints between skin cover and ribs and spars are the critical regions where high-quality bonding for intensive load transfer are required, they are hence reinforced and obviously the locations for health monitoring. The present method was developed based on this technology and hypnosis that strains in the joint regions of a composite airframe vary with the aerodynamic loadings during flight. So does the output signal of the SCF in response to the strain and loading variation that can be used to indicate the structure health status.

In addition, the sensitivity of strains from the SCF is different to different failure modes and loading conditions. For example, the occurrence of delamination in composite structure is more sensitive to compression and shear rather than tension [14]. Moreover, debonding failure is more sensitive to shear, hence torsion compared with bending moment [15]. In the scenario of unknown likely failure mode, strains collected from those SCFs in various loading cases during flight could provide adequate data for damage detection. Although the data may contain healthy or local failure information, if exists, traditional damage identification methods are not able to extract and identify the failure information from the large number of strain data samples. To this end, machine learning or deep learning algorithms have been increasingly adopted for damage classification, localization and prediction in recent years [16]. Compared with conventional machine learning algorithms for SHM, the major advantages of deep learning are the ability to automatically extract features from raw data and suitable to model large-scale data. Alvarez-Montoya et al. [17] developed an in-flight and wireless damage detection system in a UAV composite wing using strain field pattern recognition and Self-Organizing Map (SOM)-based procedure. As an unsupervised machine learning algorithm, this method can classify the damage with unlabelled dataset. Alavi et al. [18] proposed a damage detection system integrating static strain data of beam and gusset plate structures from Finite Element (FE) simulations and Probabilistic Neural Network (PNN). According to literature, the Convolutional Neural Network (CNN) model is widely utilized as a feature extractor and classifier to diagnose structural damages. Investigation into composite structure damage diagnosis using CNN based on different techniques and signals was carried out [19–24]. A damage diagnosis study using CNN fed through the strain distribution was performed and achieved high accuracy results [25]. However, the study was limited to a steel panel under tensile load case.

Although some efforts have been made in damage diagnosis using deep learning methods, the studies so far are based on simple structures and limited loading cases. There is little well received research for SHM of full-scale composite structure and taking all possible flight loading cases of an aircraft. This current study presents an investigation into damage detection and localization of a full-scale composite wing using CNN. It is practical to collect strain data of a healthy structure during flight. However, it is not feasible to collect adequate strain data samples of damaged structures for the CNN model training even in the whole service life of an airplane. Therefore, a numerical model to represent the real-life airframe must be established. In other words, a digital twin of the real-life airframe should be created and updated based on the measured strain and loading data. It can then be used to predict the failure in different modes that likely occur in the service lift of an airplane. The proposed method can be divided into four steps as depicted in Fig. 1. In step-1, aerodynamic analysis was performed to simulate the flight loadings based on an airplane design data in various flight conditions. In step-2, an FE model of the composite wing structure as part of the digital twin of the airframe was established to simulate the strain distribution in various flight loading cases. Based on the FE model of the original structure, damages in different failure modes can be simulated with the strain data at the sensor locations calculated under the same set of flight cases. In step-3, the strain data was processed as input data samples. In step-4, an end-to-end method was proposed for CNN model training to identify structural damages. In the analysis, the resulting test accuracy, uncertainty and sensitivity of the CNN models were evaluated.

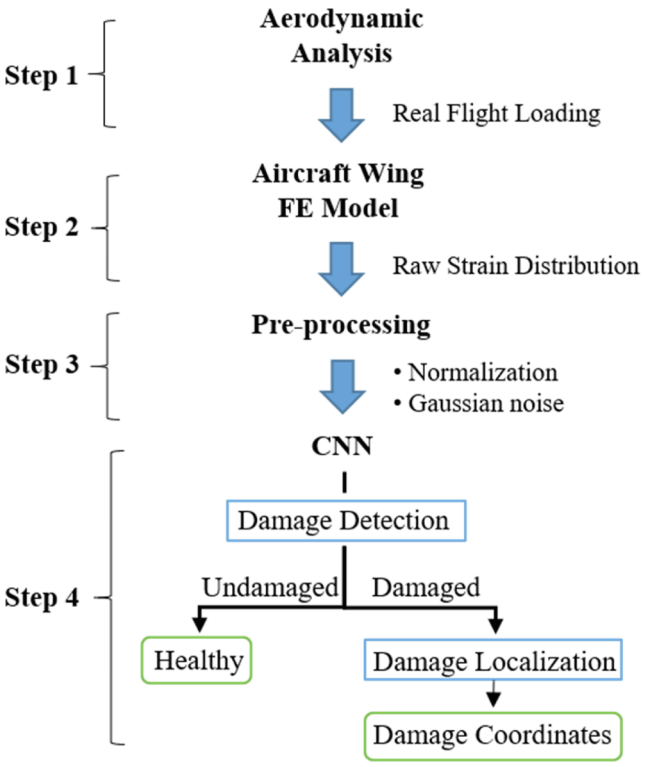


Fig. 1. Framework of the proposed method.

2. Example of numerical models

2.1. Flight load analysis

In this present study, a large civil airplane was taken as an example with the main dimensions shown in Fig. 2. The Maximum Take-Off Weight (MTOW) and Maximum Landing Weight (MLW) are 280,000 kg and 207,000 kg, respectively.

In the initial design phase, the aerodynamic loadings on the aircraft were calculated for all likely manoeuvres and flight conditions in a flight mission divided into 6 flight phases including take-off, climb, cruise, descent, approach and landing. The parameters definition for different flight conditions [26] are shown in Table 1 where the flight speed, Angle of Attack (AoA), aileron and flap deflection angles in MTOW and MLW cases were considered. This leads to over 1000 flight load cases in total. Based on the design data and flight performance requirements, a geometric model of the aircraft was created for aerodynamic load calculation using the Vortex Lattice Method (VLM) [27]. Fig. 3 shows the results of the spanwise lift force and pitching moment on the wing model

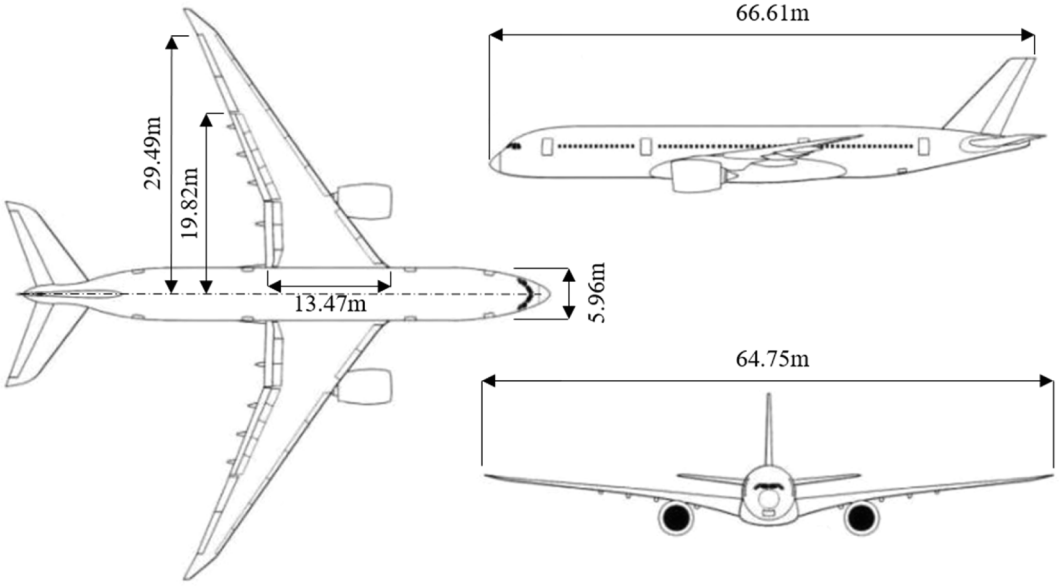


Fig. 2. An example aircraft with key dimensions taken in the study.

Table 1
Parameters definition for different flight load cases.

	MACH	AoA ()	Aileron ()	Flap ()	Weight
Take-off	0–0.3	2.4–8	0	0; 10; 15	MTOW
Climb	0.3–0.85	-0.8–1.9	0	0	MTOW
Cruise	0.85–0.89	-1–2	0; ±25; +25; -25	0	MTOW
Descent	0.3–0.85	-2–2	0; ±25; +25; -25	0	MLW
Approach	0.2–0.3	0.8–16	0	0; 20	MLW
Landing	0–0.2	-6–14	0; +25	0; 40	MLW

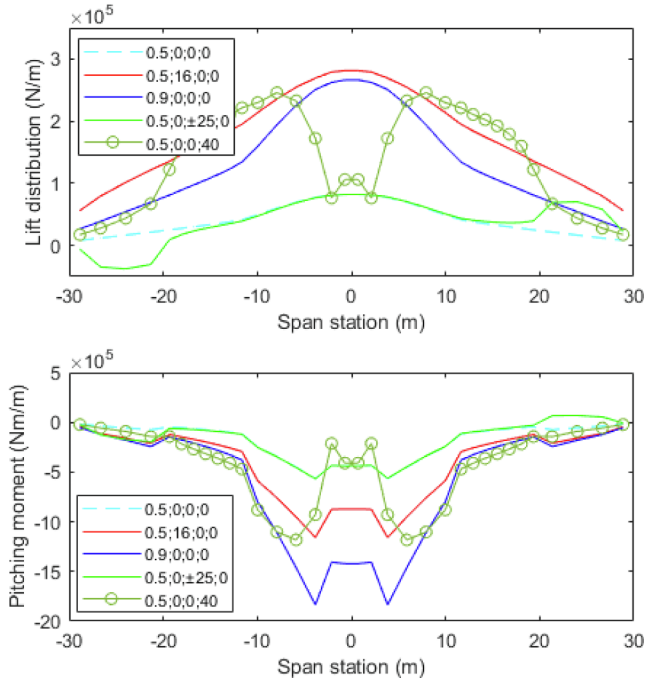


Fig. 3. The lift force and Pitching moment of the wing in five flight conditions (the values in the legend indicate the Mach number, AoA, Aileron and Flap angles).

in five of the flight cases.

2.2. FE model and analysis of the composite wing

In the FE model, the composite wing structure of the aircraft was simplified and constructed by the main structural components including the skin covers, spars, ribs and stringers as shown in Fig. 4. This model consists of 34 ribs, 34 T-section stringers and 4 rectangular section stringers. Based on the initial design, the resulting thickness of the wing skin, ribs, spars and stringers, are shown in Fig. 5. The thickness of ribs increases along the span from wingtip (1.8 mm) to maximum (20 mm) at the kink section.

Fig. 6 shows the wing geometry and mesh of the FE model. Total 13,720 2D shell elements (QUAD4) were taken with an element size of 0.17 × 0.23 m for the majority of the structure FE model. The material properties and the laminate layup and stacking sequences for each component as a result of an initial design are shown in Table 2.

3. Structure damage identification by deep learning

This section presents the training, validation and testing datasets preparation process for damage classification and localization of the composite wing structure using deep learning.

3.1. Damage models and dataset preparation

3.1.1. Damage models

The FE model of the original wing structure without damage was called as pristine structure or healthy structure (H). In order to provide data for the CNN model training, damages were created based on the original wing FE model in two different cases for investigation.

In case 1, considering the most critical structure in the kink and near the root regions of the wing, three damages were selected randomly on the upper skin of the wing in the regions. As shown in Fig. 7, the damages were modelled by the finite elements D1, D2 and D3 in the locations close to the rib 2, rib 8 and rib 10, respectively. The distance of the damaged elements D1, D2 and D3 from their nearest SCFs in the rib joint 2, 8 and 10 are 0.46 m, 0.43 m and 0.28 m, respectively. Although various numerical modelling and simulation for structure damages have been studied in previous research [28,29], the presented study was focused on the feasibility of the proposed method for SHM rather than producing an accurate damage model. In composite structure design, a

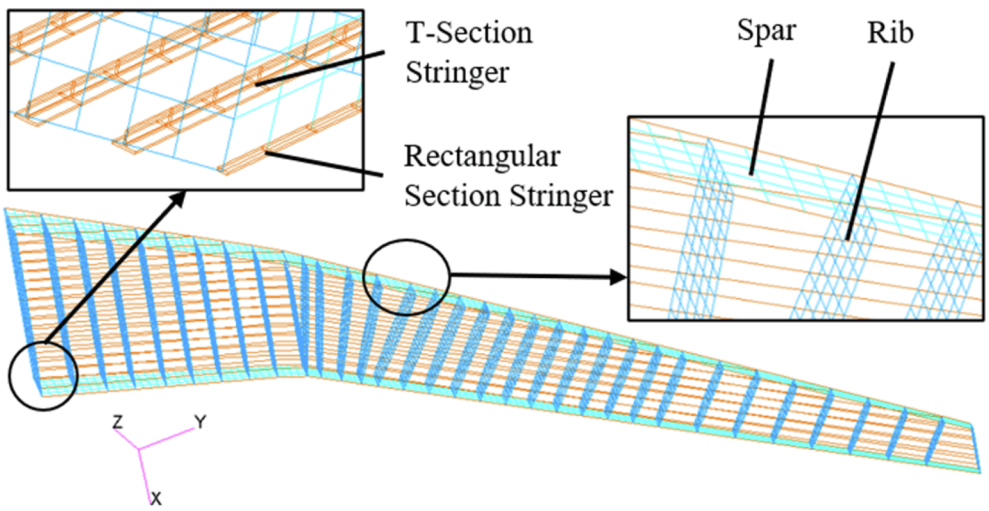


Fig. 4. The internal structure of composite wing FE model.

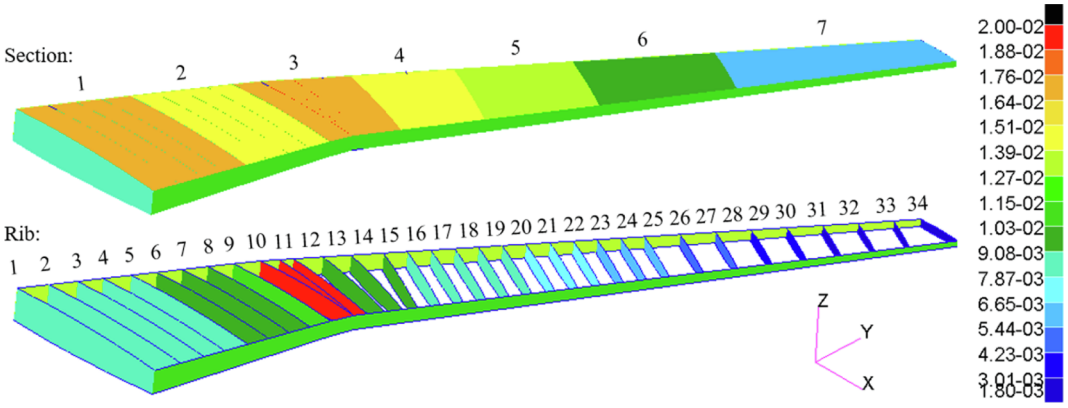


Fig. 5. Composite wing skin, rib and spar thickness (min t = 1.8 mm, max t = 20 mm).

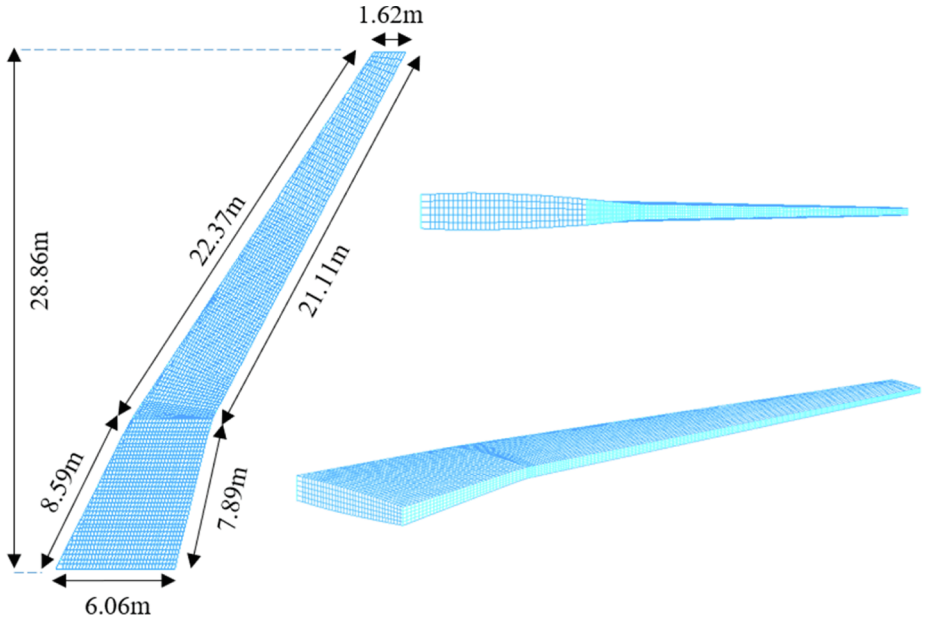


Fig. 6. Wing geometry and mesh of FE model.

Table 2
Material properties and laminate layup of the composite wing model.

Isotropic	E (GPa)		ν	
T-Section Stringer	118.9		0.31	
Rectangular Section Stringer	123.6		0.25	
Rib	79.3		0.34	
Spars and Skin Laminate	E1 = 190GPa	E2 = 17.7GPa	G12 = 6.6GPa	$\nu = 0.27$
Section	Laminate Layup			
Upper & Lower Skin (Section 1,3)	$[45/-45/0/45/0/-45/90/45/0/-45/0/45/90/-45/0/45/0/-45/0/45/0]_s$			
Upper & Lower Skin (Section 2,4)	$[45/-45/0/45/0/-45/90/45/0/-45/0/45/90/-45/0/45/0/-45/0]_s$			
Upper & Lower Skin (Section 5)	$[45/-45/0/45/0/-45/90/45/0/-45/0/45/90/-45/0/45/0/-45]_s$			
Upper & Lower Skin (Section 6)	$[45/-45/0/45/0/-45/90/45/0/-45/0/45/0/-45/0]_s$			
Upper & Lower Skin (Section 7)	$[45/-45/0/45/0/-45/90/45/0]_s$			
Front Spar	$[45/-45/0/45/0/-45/90/45/0/-45/0/45/0/-45/90/45/0/-45/0/45/90/-45]_s$			
Rear Spar	$[45/-45/0/45/0/-45/90/45/0/-45/0/45/0/-45/90/45/0/-45]_s$			

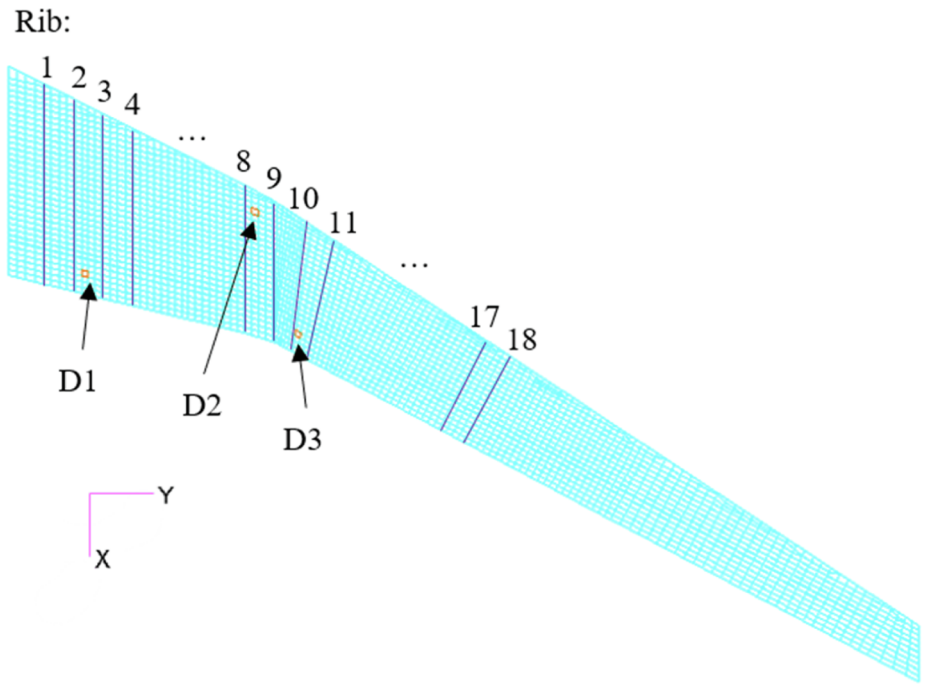


Fig. 7. Three damage locations in composite upper wing.

knockdown factor between 0.45 and 0.55 is considered based on experiment for a laminate containing a Barely Visible Impact Damage (BVID). In composite impact testing, a typical laminate sample dimension is 0.1 × 0.15 m [30]. Therefore, in the present study, the damage model was simplified by reducing the modulus (or stiffness) of the damaged elements from 20% to 80% in 20% increment. The damaged element D3 of size 0.11 × 0.16 m and reduced modulus of 40% in the wing kink region are close to the typical test sample of BVID. The damaged element D1 and D2 of size 0.17 × 0.23 m as shown in Fig. 9 with reduced modulus represent an increased damage due to compression after impact. Fig. 8 shows the resulting strain distribution of the healthy and damaged structure models under the aerodynamic forces in one of the flight cases (0.5 MACH). In this example, the modulus of the damaged element D1 was reduced by 80%. The strain variation around the damaged element is clearly noticed.

In case 2, the number of damages was increased to 28 and evenly distributed on the upper skin between the 18 skin-rib joints in the inboard wing as shown in Fig. 10. The area of each damage depends upon the local element size in the same range as the damage D1 and D3 in case 1. The damage model was created by reducing the element modulus in the range of 20%-80% in the same manner as case 1.

The wing skin-rib assembly joints usually cause critical concerns on structural integrity and overall efficiency due to geometry change and load transfer [31]. In this study, total of 324 SCFs were mounted on the upper side of the 18 skin-rib joints of the inboard wing (18 SCFs mounted in each joint) as shown in Fig. 7. In practice, a sensor would be embedded within each of the 324 SCFs to collect output signals in response to the strains acting on the SCFs during flight. However, in the present numerical simulation, the resulting average strains of the 324 elements in the SCFs locations were calculated and used to represent the sensor signals. Those extracted strain data were arranged to 18 × 18 × 1 tensor as shown in Fig. 9 as input data for the CNN model training. The strain data was then normalized to make all the parameters into the range [0,1] and transformed into grayscale images, which was used as input to feed the CNN architecture.

3.1.2. Data preparation for damage case 1

Furthermore, four groups of datasets of different flight load cases and data samples as listed in Table 3 were considered to evaluate their influence on the analysis results. For Dataset 1 and Dataset 2 scenarios, the

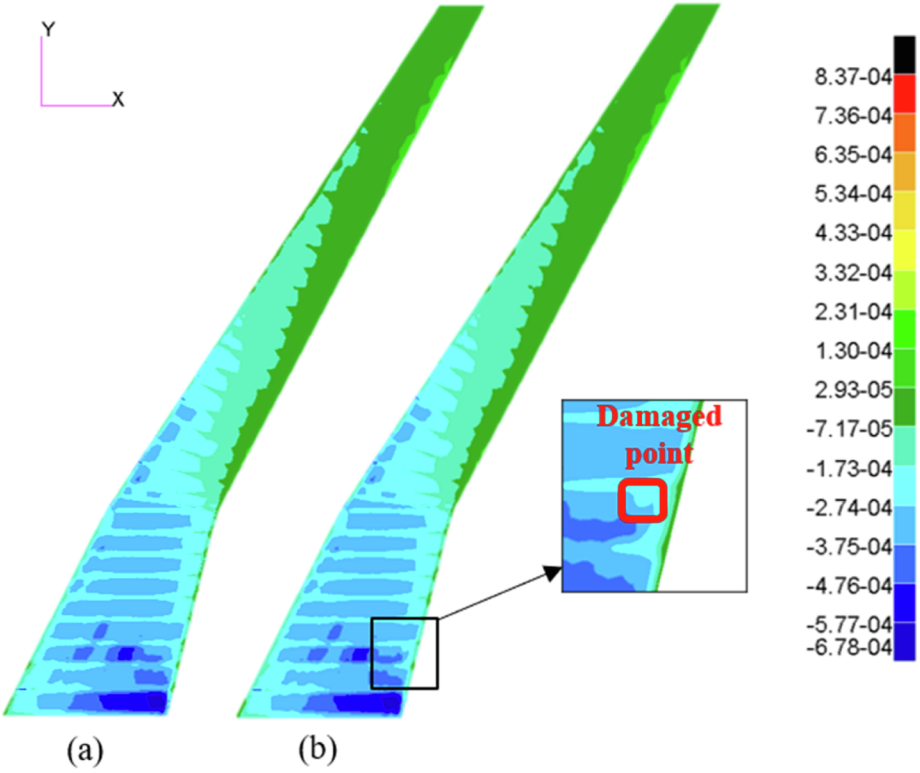


Fig. 8. Strain distribution in span-wise direction for (a) pristine structure and (b) damaged structure (D1 of stiffness reduced by 80%) at aircraft speed 0.5 MACH.

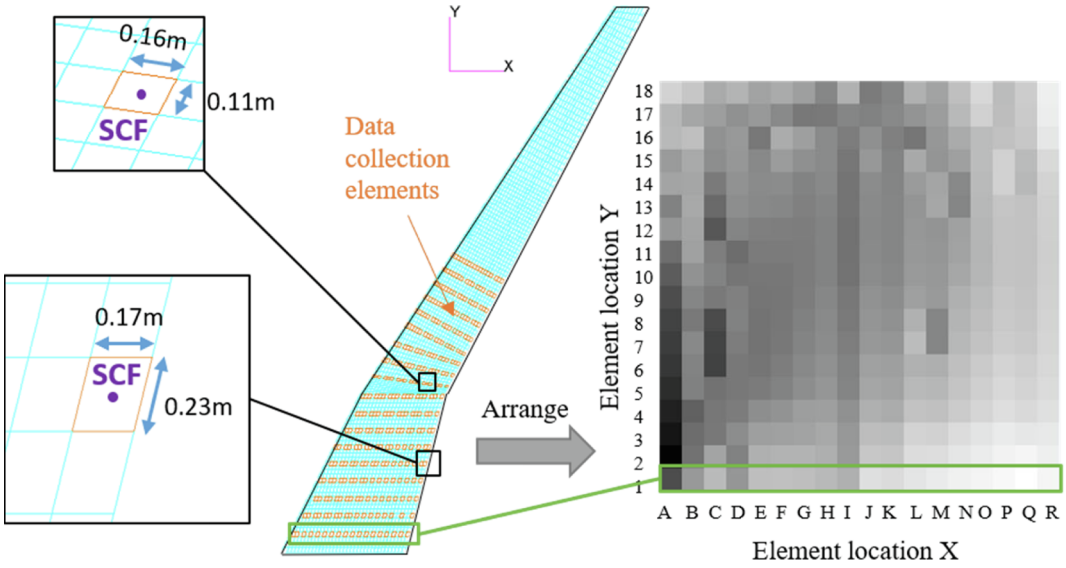


Fig. 9. Sensor locations and pre-processing of CNN input data.

damaged element D1, D2 and D3 modulus were reduced by 80% in the structure for analysis in all flight cases. In the 'H' (healthy) structure in the noise-free scenario, there were 1000 flight load cases and 324 strain data in the sensor locations available for model training and testing. For the 'H' and 3 damage (D1, D2, D3) scenarios, a dataset of total 4000 × 324 was obtained. To simulate the noise due to environmental effects in practice, a randomly generated white Gaussian noise (AWGN, $N(0,\sigma^2)$), where σ^2 is the variance of the measurement noise was introduced in the training, validation and testing datasets. Four different noise levels (0.5%, 1%, 1.5% and 2%) were added to the original Dataset 1 samples for model training only, while Dataset 2 samples remain noise-free during training. To evaluate the sensitivity of the method to different damage severities, damage D1 of four different damage severities (modulus reduced by 80%, 60%, 40% and 20%) were set in Dataset 3 to compare with the 'H' model using the noise-free data samples in all flight load cases. To reduce the influence of different flight conditions on strain distribution variation and improve the damage detection accuracy, the data samples used in Dataset 4 were collected from only the Landing phase.

For Dataset 1, Dataset 2 and Dataset 4, the trained models were tested 10 times with test data samples including different noise levels (0%, 0.4%, 0.8%, 1.2%, 1.6% and 2%). Noise level denotes the ratio between the standard deviation of measurement noise to the actual

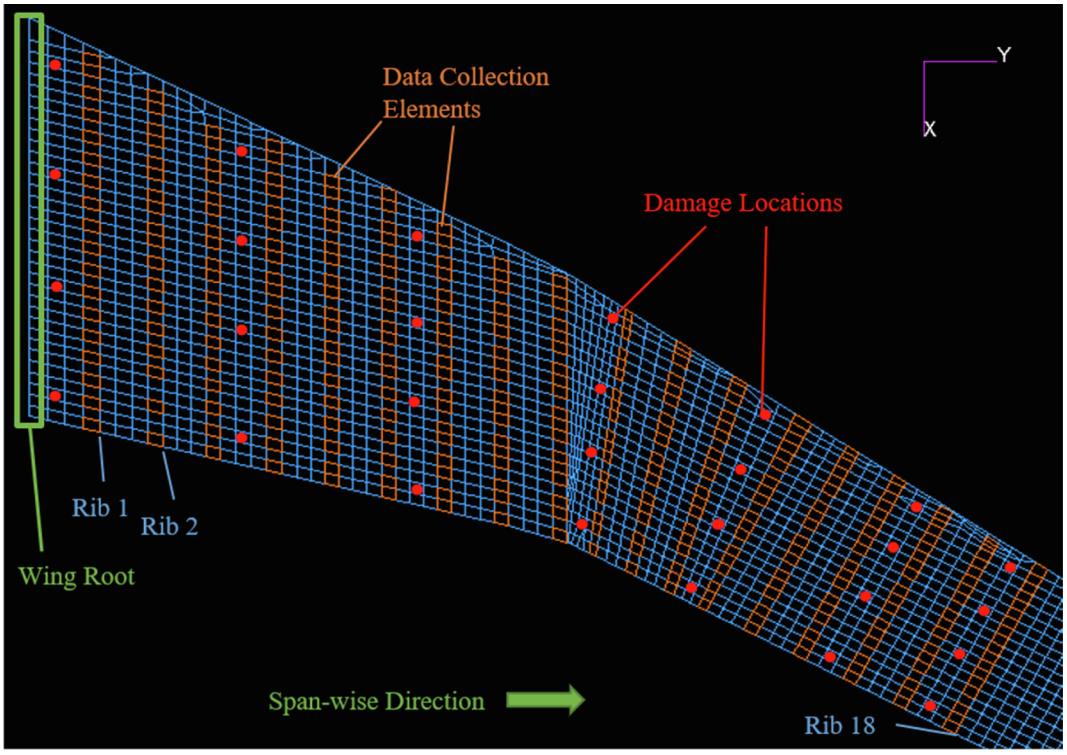


Fig. 10. Damage locations for damage localization task.

Table 3
Details of the four datasets.

	Stiffness Reduction	Load Case	Noise Level (%)	Class	Total samples
Dataset 1:	80%	All flight phases/ 1000	0, 0.5, 1, 1.5, 2	H, D1, D2, D3	20,000
Dataset 2:	80%	All flight phases/ 1000	0	H, D1, D2, D3	4000
Dataset 3:	20%,40%,60%,80%	All flight phases/ 1000	0	H, D1	8000
Dataset 4:	80%	Landing/ 656	0	H, D1, D2, D3	2624

strain values. For Dataset 3, trained models were tested with noise-free samples. None of the loading scenarios of training datasets was used in the testing. It is a common practice to randomly split the data into training, validation and testing sets in machine learning models. Fig. 11 shows the number of load cases for neural network training, validation, and testing. Dataset 1 and Dataset 2 were randomly split by a ratio of 6:2:2. Dataset 3 was randomly split by a ratio of 8:1:1. Dataset 4 contains 500 training sets, 100 validation sets and 56 testing sets. All the 4 groups of data were trained, validated and tested in CNN models, which will be illustrated in the next section.

3.1.3. *Data preparation for damage case 2*

Except for damage detection, localizing the damage is also a key issue for SHM. In Dataset 5, the damage locations of each damage and the strain data were both collected for the damage localization task. In Fig. 10, the red points represent the 28 damage locations, and the orange rectangles represent 324 strain data collection elements. The coordinates of each damage location were stored as a bounding box in an order of (y,x,w,h), where x and y indicate the coordinate of the upper left node of a damaged element, w and h define the width and length of the damaged element. For example, the bounding box of the four damage locations in the first column were defined as (1,2,2,2), (1,7,2,2), (1,12,2,2) and (1,17,2,2) respectively. While the damage locations in the second column were defined as (4,2,2,2), (4,7,2,2), (4,12,2,2) and (4,17,2,2) respectively. By analogy, the damage locations in the last column were defined as (18,2,2,2), (18,7,2,2), (18,12,2,2) and (18,17,2,2).

In damage localization task, the CNN was trained with the data collected from the Climb Phase. Hence, 64 loading scenarios were used.

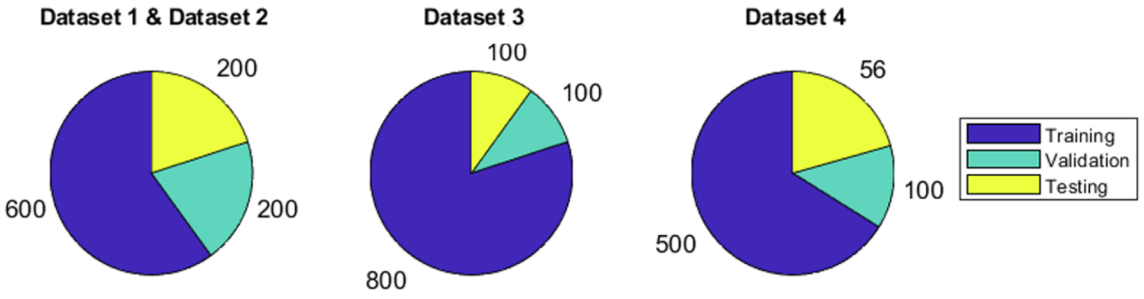


Fig. 11. Load cases for CNN training, validation and testing.

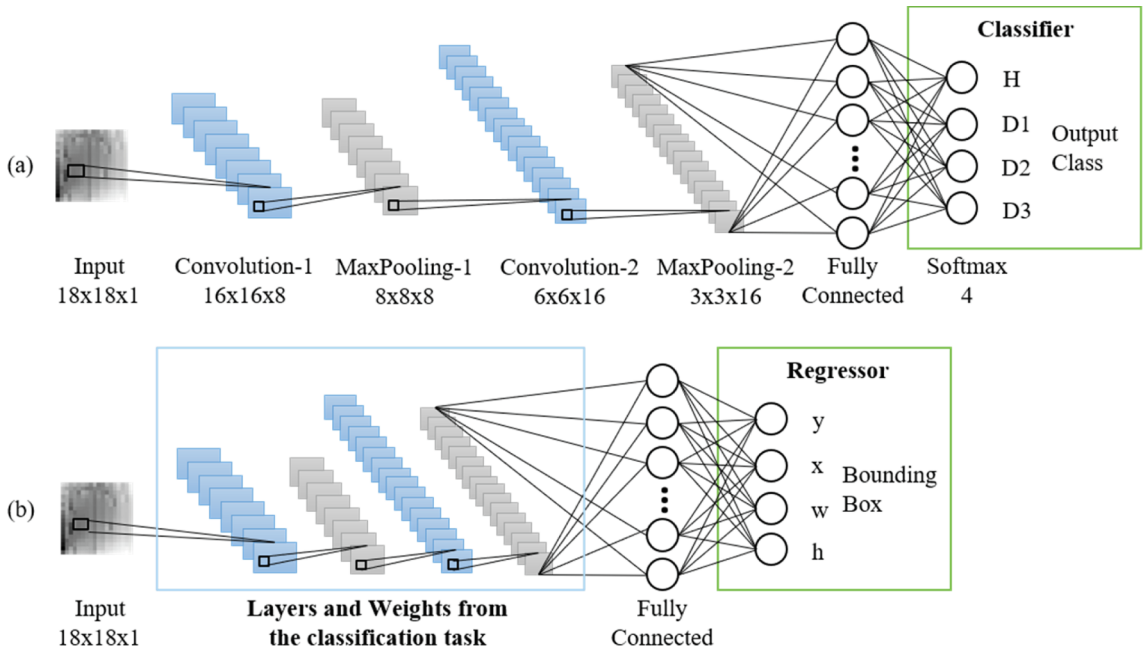


Fig. 12. Proposed architecture of CNN for (a) damage classification task (b) damage localization task.

All the damage scenarios were simulated by reducing the stiffness of an element by 80%. In this section, the neural network was trained, validated and tested with noise-free data. As a result, a total of 1792 damaged samples were generated in Dataset 5. Dataset 5 was randomly split into training, validation and testing datasets by a ratio of 8:1:1.

3.2. CNN architectures

The framework of CNN was firstly proposed by LeCun [32] for the task of classifying images of handwritten digits. After years of development, the performance of this method has dramatically improved. It has proven to be a very efficient structure for image recognition, speech recognition, object detection and many other domains. For a given input instance, this method tries to build a prediction function parametrized by weights. The loss function is used to measure the error between the true value and the prediction. The training process is consisting of feedforward and backpropagation [33]. The feedforward process evaluates the prediction function. After that, the backpropagation process adjusts the weights according to their contribution to the error by using the Stochastic Gradient Descent (SGD) algorithm. The parameters were updated with the learning rate. The learning process was to seek the best prediction function and best possible values of weights to minimize the loss function [34].

CNNs receive the input in the form of multiple arrays: one-dimensional (1D) volumes for signals; 2D for images or audio and 3D for volumetric images or video. CNNs are featured by four key properties: local connections; shared weights; subsampling and many layers [35]. Typically, the structures of CNNs are composed of the filter stage and classification stage (or regression stage). The filter stage is formed by stacking convolutional layers, activation layers and pooling layers. The main objective of the convolutional layer is to extract features by sliding a filter or kernel over small patches of the image from the input image. An activation layer, such as the Rectified Linear Unit (ReLU), follows the convolution operation. The pooling layer is employed to reduce the resolution of the feature maps by performing a down-sampling operation. To achieve better performance, batch normalization layers can also be employed between convolutional layers and activation layers. The convolutional and pooling layers are followed by one or more fully-connected layers. The damage detection task treats the case as a classification problem where the goal is to determine the presence of damage. The damage localization task estimates the location of the damage where it is treated as a regression problem. Different prediction functions and loss functions were adopted for the classification task and localization task.

It is important to select appropriate loss functions to converge and optimize the proposed model. Two different loss functions were adopted for the damage detection and localization tasks. The detection part employed the cross-entropy loss. The formula of cross-entropy loss is shown below:

$$\mathscr{L}_c = -\sum_{i=1}^{N}\sum_{c=1}^{M} t_{ic}\ln p_{ic} \tag{1}$$

where N and M indicate the number of samples and classes, t_{ic} is the indicator that the i-th sample belongs to the c-th class, p_{ic} is the value of probability prediction from the softmax function.

The regression part computes the loss between the predicted and the true bounding box with the Mean Squared Error (MSE), which is the $\mathscr{L}_2$ loss function.

$$\mathscr{L}_2 = \sum_{i=1}^{N}\frac{(t_i - \hat{t}_i)^2}{N} \tag{2}$$

where t_i represents the target output and $\hat{t}_i$ is the network's prediction for sample i. During the regressor training process, if the predicted bounding box satisfied the conditions of Equation (3), the damage location was marked as correct.

$$\begin{aligned} |y-\hat{y}| &< thr \\ |x-\hat{x}| &< thr \\ |w-\hat{w}| &< thr \\ |h-\hat{h}| &< thr \end{aligned} \tag{3}$$

where $(\hat{y}, \hat{x}, \hat{w}, \hat{h})$ is the predicted damage location, (y, x, w, h) is the true damage location, thr is the threshold.

Deep learning models are full of hyperparameters and finding the best configuration for these parameters can improve the performance of the neural networks [36]. The architectures of CNN can be built in

Table 4
Proposed network configuration for Dataset 1, Dataset 2 and Dataset 4.

Layer Name	Layer Description
Input	18 × 18 × 1 Image
Convolution-1	Filter size (3 × 3), Stride 1, Number of Filter 8, Batch Normalization, ReLU
MaxPooling-1	Filter size (2 × 2), Stride 2
Convolution-2	Filter size (3 × 3), Stride 1, Number of Filter 16, Batch Normalization, ReLU
MaxPooling-2	Filter size (2 × 2), Stride 2
Fully-connected, Softmax	Output = 4

various ways by stacking convolutional layers, pooling layers and fully-connected layers. The hyperparameters include the number of convolutional layers and fully-connected layers, the number of kernels (2 to 2^7), kernel size (3*3 or 5*5) and pool size (1*1 with stride of 1 or 2*2 with stride of 2), learning rate (2 to 2^{-8}), batch size, and randomly selected hidden layer sizes.

The learning rate is one of the most important hyperparameters, which controls the amount of the updated weights during neural network training. In general, the larger the learning rate the quicker the training process, although it may result in a sub-optimal final set of weights. A smaller learning rate may allow the model to gain more optimal set of weights, but may need significantly larger training epochs. If the learning rate is too small, the training may never converge or stuck in a suboptimal solution. Therefore, an appropriately configured learning rate is important for the neural network model to achieve good performance in a given number of training epochs.

Fig. 12 (a) shows the proposed architecture for Dataset 1, Dataset 2 and Dataset 4. The network was composed of two convolutional and pooling layers for automatically extracting features from the healthy and damaged cases. Fully-connected and softmax layers were used to classify the inputs as Healthy (H), Damage 1 (D1), Damage 2 (D2) and Damage 3 (D3) cases. The weights were initialized randomly and trained from scratch. The learning rate was set to 0.01. In this paper, a batch size of 64 was implemented in the training process for all the CNN models. Table 4 summarises the details of the proposed CNN architecture in Fig. 12 (a).

The proposed network for Dataset 3 was composed of two convolutional layers and one maxpooling layer. The kernel size of the convolutional layer was set to 3 × 3. The number of kernels was 8 and 16 respectively. Pool size 2 × 2 with a stride of 2 was used for the pooling layer. The last convolutional layer was connected to one fully-connected layer. The softmax layer outputted two structural conditions: Healthy (H) and Damaged 1 (D1). The weights were initialized randomly. The learning rate was set to 0.0026. This model was trained, validated and tested in four different damage severities (stiffness reducing 20%, 40%, 60% and 80%).

The architecture of the regression neural network in Fig. 12 (b) was converted from the classification neural network in Fig. 12 (a). The CNN architecture for localization task (Dataset 5) replaced the fully-connected layer, softmax layer and classification layer with a fully-connected layer of size 4 and a regression layer. The weights for the regression neural network were initialized using the weights from the classification neural network. Keeping the layers and weights from the classification task can significantly speed up the network training. In this CNN model, the learning rate of 0.001 was adopted. The threshold values 1.5, 2 and 2.5 were selected for *thr* described in Equation (3) to discover the damage localization accuracy. The results are illustrated in the next section.

4. Results and discussion

4.1. Damage classification task

This section presents the performance of the proposed methodology for damage classification task. For Dataset 1, Dataset 2 and Dataset 4, the models were trained for up to 10 epochs. Fig. 13 shows the detailed classification results of the CNN models on the testing data with confusion matrixes. The vertical axis shows the true classes, while the horizontal axis shows the predicted labels assigned by CNN classifier. Confusion matrix visualizes the testing results and shows the testing accuracy for each class. Fig. 13 (a-d, g, h) shows the results of Dataset1, Dataset 2 and Dataset 4 with the testing data noise levels of 0% and 2%, respectively. In Fig. 13 (a, c, g), the overall prediction accuracies for the three datasets are 99.9%, 94.4% and 97.8%, respectively. The major loss of accuracy was mainly due to misclassifying the H and D2 cases.

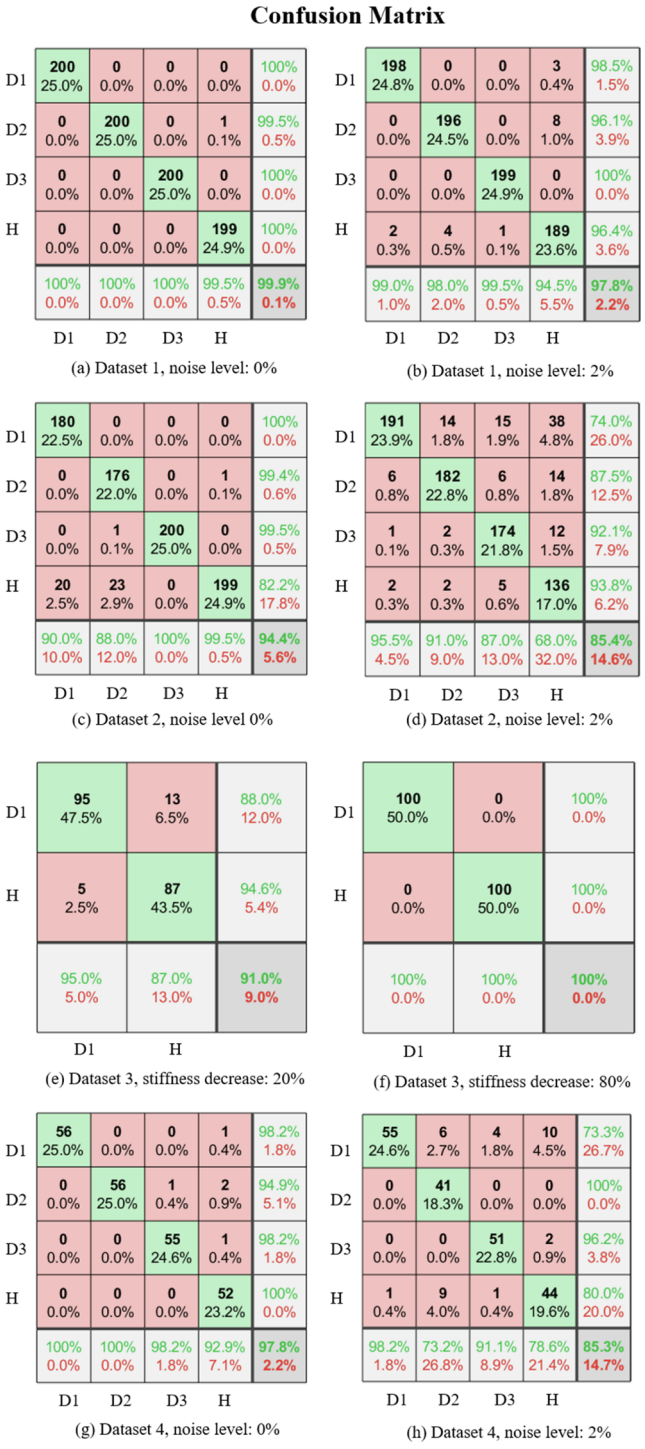


Fig. 13. Confusion matrixes of CNN in damage classification.

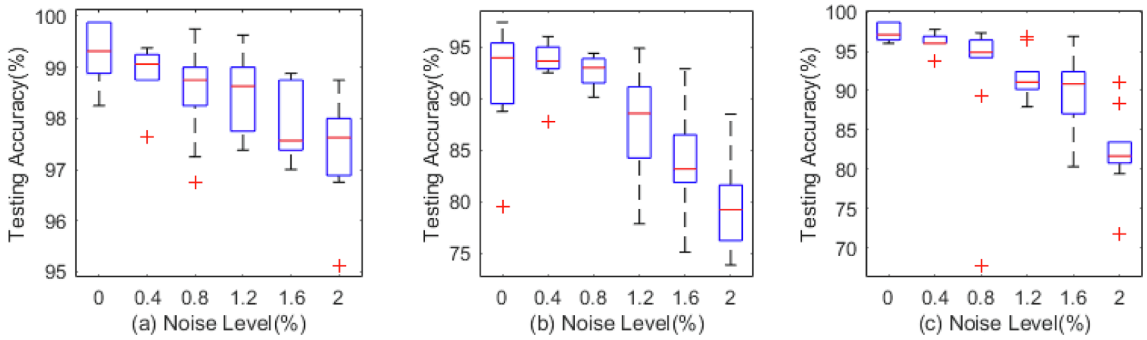


Fig. 14. Testing accuracy of damage classification task trained with (a) Dataset 1, (b) Dataset 2 and (c) Dataset 4.

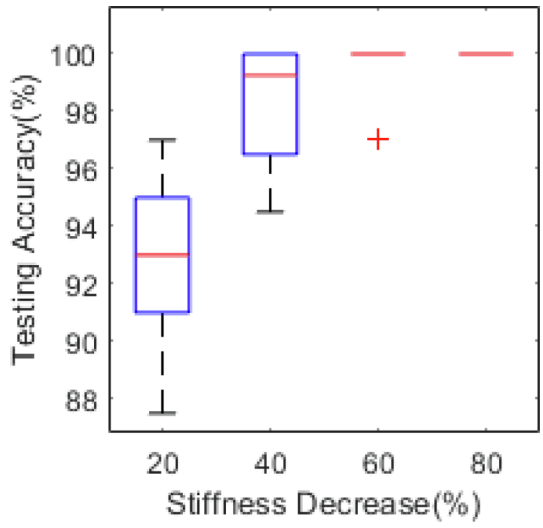


Fig. 15. Testing accuracy of damage classification result in four different damage severities (Dataset 3).

Specifically, 5.1% examples of the D2 case were misclassified in Dataset 4, out of which 1.5% were misclassified as D3, 3.6% were misclassified as H. Similarly, 9.5% examples of the H cases were misclassified as D2 in Dataset 2, and 0.5% of the D2 cases were misclassified as H in Dataset 1. The misclassification results are consistent with the physics of the problem, because the strain at D2 is smaller than D1 and D3 in the wing structure. Hence, the H case and D2 case may have the same response to certain loading conditions. However, when increasing the noise level from 0% to 2%, the major loss of accuracy was mainly due to noise. Fig. 13 (e, f) presents the results of Dataset 3 with the material stiffness decreased 20% and 80%, respectively. The damaged areas are the same for the two cases. More severe damage causes greater changes in the strain of the structure. Thus, the overall classification accuracy increased from 91% to 100%. In general, the results above demonstrate the feasibility of CNN models in damage classification task on the given datasets.

As the deep learning models perform successfully on all the four datasets, Dataset 1, Dataset 2 and Dataset 4 were selected to analyse the uncertainty of the model. Adding various levels of noise to the data to simulate the environmental effects and measurement noise enhances the reliability of the proposed method. The accuracy and robustness of the CNN model are discussed. Fig. 14 presents the testing accuracy for Dataset 1, Dataset 2 and Dataset 4 in damage classification task. Herein, the horizontal axis shows the noise level of the testing data, while the vertical axis shows the damage classification accuracy of each case after testing 10 times. Fig. 14 (a) presents the best testing performance among the given training cases. According to the figure, the proposed architecture classified the four cases with 99% accuracy for noise-free data.

Table 5
Examples of bounding box predicted by CNN.

Case	True Damage Location	Predicted Damage Location	Error ($\lvert Predicted - True \rvert$)
1	(7, 17, 2, 2)	(8.8, 16.9, 2.1, 1.9)	(1.8, 0.1, 0.1, 0.1)
2	(16, 7, 2, 2)	(15.3, 7.5, 2.1, 1.9)	(0.7, 0.5, 0.1, 0.1)
3	(10, 2, 2, 2)	(10.6, 2.9, 1.9, 1.9)	(0.6, 0.9, 0.1, 0.1)
4	(16, 2, 2, 2)	(15.4, 2.5, 2.0, 1.9)	(0.6, 0.5, 0, 0.1)
5	(1, 12, 2, 2)	(1.0, 10.6, 2.1, 2.2)	(0, 1.4, 0.1, 0.2)

The high accuracy represents the proposed methodology is capable of learning the damage features. It is noticeable that the testing accuracy decreases with the increase of the noise levels. However, the testing accuracy remained above 97% under 2% noise level, which illustrates that the CNN is robust for various levels of noise. The testing accuracies of Fig. 14 (b) are lower than Fig. 14 (a). The testing accuracy was 94% for noise-free data, but it dropped to 79% for the noise level of 2%. Hence, adding different levels of noise in the training process helped the neural network to learn damage features under uncertainty. Then, the training, validation and testing dataset was segmented according to flight status. For example, Dataset 4 was composed of data only collected from the landing phase. It is noticeable that the testing accuracy in Fig. 14 (c) is higher than in Fig. 14 (b). This is because the damage condition in this study is simulated by reducing the element stiffness, the resulting damage mode is sensitive to all flight conditions. The neural network training based on the flight conditions can help to reduce the variation of strain distribution due to load differences. For different types of damage modes however, some damage modes may be insensitive to a specific load condition and affect the damage detection results.

Dataset 3 was used to analyse the sensitivity of the model. The CNN classifier was employed to predict labels for cases under four different damage severities (stiffness reduced by 20%, 40%, 60% and 80%). For example, Fig. 15 displays the testing accuracy of detecting the damage D1 of different damage severity after testing 10 times based on the model trained for up to 100 epochs. The results show that the testing accuracy was 93% for the smallest damage D3 (modulus reduced by 20%), and became 99% when the damage severity increased with modulus reduced by 40%; the testing accuracy reached 100% when the element modulus was reduced by larger than 60%. Since the more severe the damage, the more likely to be detected, the testing accuracy provides an indicator for the damage severity apart from damage detection accuracy by using the method.

4.2. Damage localization task

The CNN model was further employed to predict the coordinate of the damages. This section trained the CNN model with Dataset 5, which was collected from the Climb Phase. As described in Section 3.1.3, the strain information for 324 data acquisition points were extracted for the analysis. 28 damage locations and 64 loading scenarios were considered.

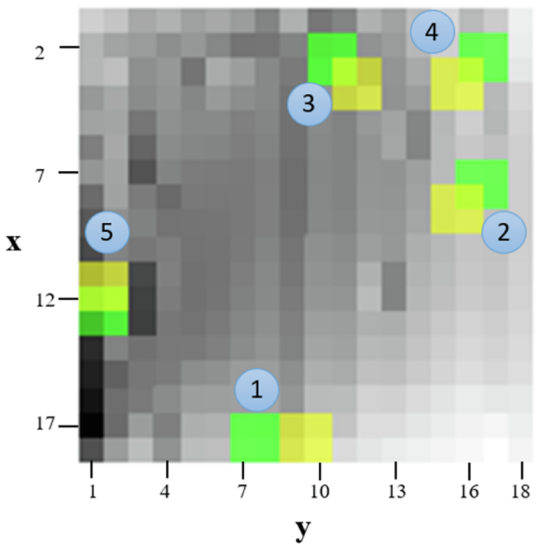


Fig. 16. Damage location estimation of 5 cases in Table 5 (green box: true damage location; yellow box: predicted damage location).

The model was trained for up to 50 epochs. Then, the trained model was tested with noise-free data. Table 5 gives five examples of bounding boxes predicted by CNN and compares the errors between the true damage locations and the predicted locations as well. Fig. 16 visualized the damage localization results by plotting the true damage location in green box and the predicted damage location in yellow box.

Fig. 17 shows a representative result of the testing errors at each damage location for localization task. Herein, the x-axis and y-axis show the value of x and y in the bounding box of the testing data respectively, while the z-axis shows the testing errors. In Fig. 17 (a), the proposed method localized the damage with 83% overall accuracy when the threshold value was 1.5 (thr = 1.5). When the threshold values were 2 (Fig. 17 (b) thr = 2) and 2.5 (Fig. 17 (c) thr = 2.5), the overall accuracy increased to 95% and 99% respectively. As it is seen, the proposed model has better performance in predicting the damages at the central position than at the edge. The reason for this may be that there are fewer data acquisition points at the edge to monitor the health condition of the structure than at the centre. Reorganizing the distribution and number of the data acquisition points can be a potential strategy for increasing the damage diagnosis precision.

The CNN model was tested 10 times with randomly selected training, validation and testing data to localize the damage. Fig. 18 shows the overall testing accuracy when the threshold values were 1.5, 2 and 2.5.

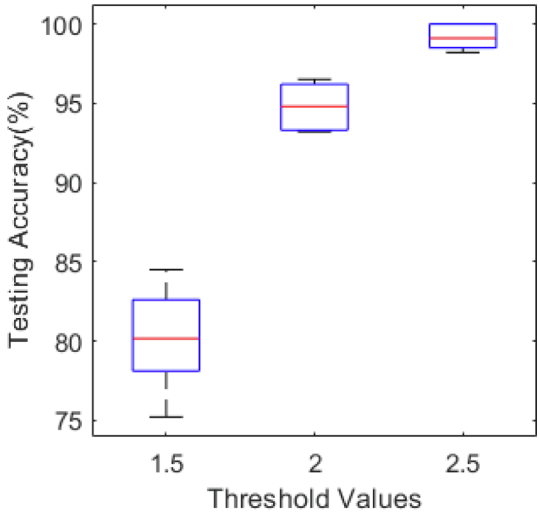


Fig. 18. Performance analysis of localization task for thresholds 1.5, 2 and 2.5.

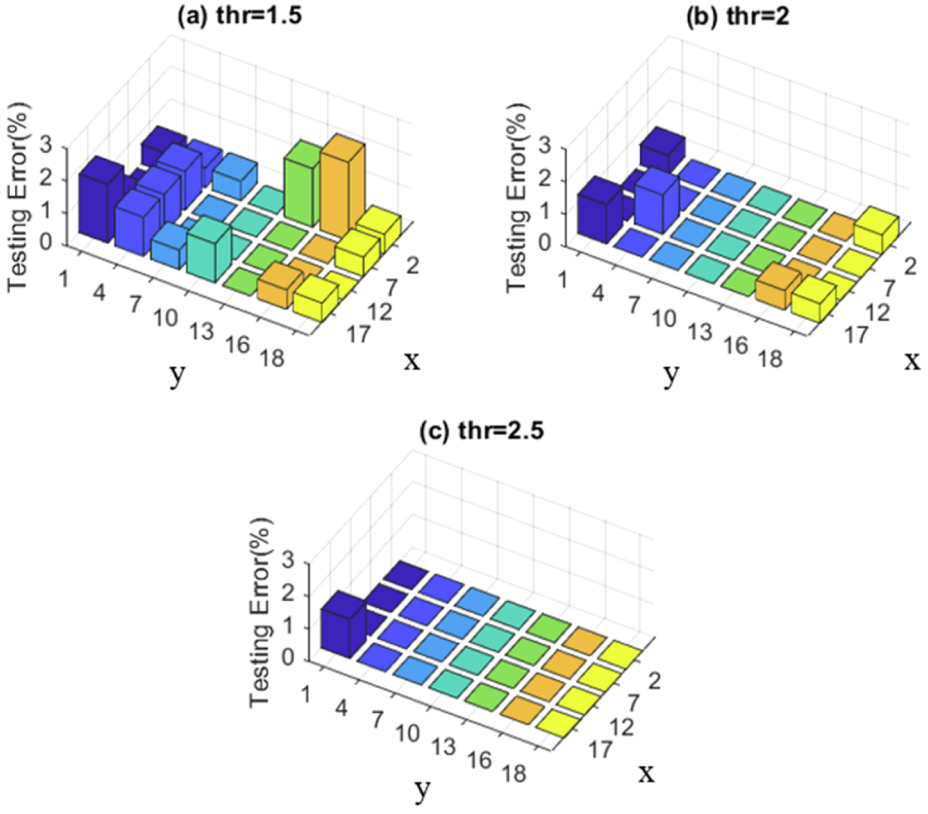


Fig. 17. Damage localization task testing errors at each damage location for thresholds: (a) thr = 1.5; (b) thr = 2; (c) thr = 2.5.

When the damage location was searched in the larger region by increasing the threshold, the accuracy rate was increased obviously. The testing accuracy was almost 99% for threshold value 2.5. The high overall localization accuracy demonstrates that the proposed method can successfully predict the damage locations. However, the CNN model cannot give a visible function to describe the relationship between the input strain data and the output results, though it can classify the structural health condition and predict the damage locations. This is because the characteristic of a deep learning model is to find the relationship between the inputs and outputs by constructing complicated layers. These layers make the model possible to fit the datasets. However, it also makes the deep learning model too complicated to give a visible function.

5. Conclusion

An investigation into a proposed CNN-based data-driven SHM method is demonstrated by numerical analysis using the strain data to represent a network of 324 sensors output from the skin-rib joints of an aircraft composite wing in response to various flight loads. In this method, all parameters of the CNN model were jointly trained hence suitable for large-scale data. Based on the investigation, some conclusions can be drawn below.

- The damage features of a structure are included and remain in the strain data for different loading cases in an aircraft flight mission. The features can be identified by employing the CNN-based method to classify the structural health conditions based on the strain data samples in different flight loading cases.
- The introduction of system noise can avoid overfitting and lead to a better testing performance to improve the reliability of the method. In the case of noise (2%) existing in the data samples used for CNN model training and testing, the reduction of testing accuracy of the structural damage is negligible. In the case of noise-free data for training only, the testing accuracy can be reduced by about 13% for 2% noise existing in the data samples for testing.
- The sensitivity of the damage classification task can be used to evaluate the damage severity. Furthermore, the pre-trained CNN regressor can be used to localize the damages. The performance of the damage localization task can be evaluated according to the damage locations and threshold values. The method shows an overall damage localization accuracy of 83% for the threshold value of 1.5.
- The damages occurring in the middle of the wing structure can be better detected with smaller testing errors than the damages near the junction of skin and the front and rear spars.
- The CNN performance highly depends on the training dataset; hence the accuracy and robustness of the model can be improved by increasing the samples in the training dataset.
- This proposed CNN-based SHM method is of high accuracy in structure damage classification and localization tasks and demonstrates its feasibility for application.

CRediT authorship contribution statement

Minxiao Lin: Formal analysis, Data curation, Software, Writing – original draft, Writing – review & editing. **Shijun Guo:** Conceptualization, Methodology, Validation, Writing – review & editing. **Shun He:** Software. **Wenhao Li:** Writing – review & editing. **Daqing Yang:** Software.

Declaration of Competing Interest

The authors declare that they have no known competing financial interests or personal relationships that could have appeared to influence the work reported in this paper.

Acknowledgement:

The authors acknowledge the financial support from the National Natural Science Foundation of China (NSFC No. 11972079 & 12102317).

References

[1] Pervaiz M, Panthapulakkal S, Kc B, Sain M, Tjong J. Emerging trends in automotive light-weighting through novel composite materials. Mater Sci Appl 2016;07(01):26–38.
[2] Guo S, Li W. Numerical analysis and experiment of sandwich T-joint structure reinforced by composite fasteners. Compos Part B Eng 2020;199:108288.
[3] Rana S, Subramani P, Fangueiro R, Correia AG. A review on smart self-sensing composite materials for civil engineering applications. AIMS Mater Sci 2016;3:357–79. https://doi.org/10.3934/matersci.2016.2.357.
[4] Gupta G, Kumar A, Tyagi R, Kumar S. Application and future of composite materials: a review. Int J Innov Res Sci Eng Technol 2016;5:6907–11.
[5] Li W, Guo S, Giannopoulos IK, He S, Liu Y. Strength enhancement of bonded composite laminate joints reinforced by composite Pins. Compos Struct 2020;236:111916. https://doi.org/10.1016/j.compstruct.2020.111916.
[6] Naebe M, Abolhasani MM, Khayyam H, Amini A, Fox B. Crack damage in polymers and composites: a review. Polym Rev 2016;56(1):31–69. https://doi.org/10.1080/15583724.2015.1078352.
[7] Soleimanpour R, Ng CT. Locating delaminations in laminated composite beams using nonlinear guided waves. Eng Struct 2017;131:207–19. https://doi.org/10.1016/j.engstruct.2016.11.010.
[8] Mizuno Y, Hagiwara S, Lee H, Ochi Y, Matsui T, Matsumoto Y, et al. Infrared thermometry for breakage detection of optical fibers embedded in structures. Appl Phys Express 2019;12(6):062007. https://doi.org/10.7567/1882-0786/ab1e92.
[9] Güemes A, Fernández-López A, Díaz-Maroto PF, Lozano A, Sierra-Perez J. Structural health monitoring in composite structures by fiber-optic sensors. Sensors 2018;18:1–11. https://doi.org/10.3390/s18041094.
[10] Seguel F, Meruane V. Damage assessment in a sandwich panel based on full-field vibration measurements. J Sound Vib 2018;417:1–18. https://doi.org/10.1016/j.jsv.2017.11.048.
[11] Guo S, Hemingway NG. An orthogonality sensitivity method for analytical dynamic model correction using modal test data. J Sound Vib 1995;187(5):771–80. https://doi.org/10.1006/jsvi.1995.0562.
[12] Guo S, Hemingway NG. An energy error estimation method for improving analytical models using vibration modal test data. Proc Inst Mech Eng Part C J Mech Eng Sci 1995;209(2):97–105. https://doi.org/10.1243/PIME_PROC_1995_209_129_02.
[13] Li W, Guo S, Giannopoulos IK, Lin M, Xiong Y, Liu Y, et al. 3D-printed thermoplastic composite fasteners for single lap joint reinforcement. Compos Struct 2022;282:115085. https://doi.org/10.1016/j.compstruct.2021.115085.
[14] Malhotra A, Guild FJ. Impact damage to composite laminates: effect of impact location. Appl Compos Mater 2014;21:165–77. https://doi.org/10.1007/s10443-013-9382-z.
[15] Zimmermann N, Wang PH. A review of failure modes and fracture analysis of aircraft composite materials. Eng Fail Anal 2020;115:104692. https://doi.org/10.1016/j.engfailanal.2020.104692.
[16] Zhao R, Yan R, Chen Z, Mao K, Wang P, Gao RX. Deep learning and its applications to machine health monitoring. Mech Syst Signal Process 2019;115:213–37. https://doi.org/10.1016/j.ymssp.2018.05.050.
[17] Alvarez-Montoya J, Carvajal-Castrillón A, Sierra-Pérez J. In-flight and wireless damage detection in a UAV composite wing using fiber optic sensors and strain field pattern recognition. Mech Syst Signal Process 2020;136:106526. https://doi.org/10.1016/j.ymssp.2019.106526.
[18] Alavi AH, Hasni H, Lajnef N, Chatti K, Faridazar F. An intelligent structural damage detection approach based on self-powered wireless sensor data. Autom Constr 2016;62:24–44. https://doi.org/10.1016/j.autcon.2015.10.001.
[19] Li X, Li J, Qu Y, He D. Gear pitting fault diagnosis using integrated CNN and GRU network with both vibration and acoustic emission signals. Appl Sci 2019;9:768. https://doi.org/10.3390/app9040768.
[20] Abdeljaber O, Avci O, Kiranyaz S, Gabbouj M, Inman DJ. Real-time vibration-based structural damage detection using one-dimensional convolutional neural networks. J Sound Vib 2017;388:154–70. https://doi.org/10.1016/j.jsv.2016.10.043.
[21] Cha Y-J, Choi W, Büyüköztürk O. Deep learning-based crack damage detection using convolutional neural networks. Comput Civ Infrastruct Eng 2017;32(5):361–78.
[22] Abdeljaber O, Avci O, Kiranyaz MS, Boashash B, Sodano H, Inman DJ. 1-D CNNs for structural damage detection: verification on a structural health monitoring benchmark data. Neurocomputing 2018;275:1308–17. https://doi.org/10.1016/j.neucom.2017.09.069.
[23] Lin Y-Z, Nie Z-H, Ma H-W. Structural damage detection with automatic feature-extraction through deep learning. Comput Civ Infrastruct Eng 2017;32(12):1025–46.
[24] Xu L, Yuan SF, Chen J, Bao Q. Deep learning based fatigue crack diagnosis of aircraft structures. In: Proc 7th Asia-Pacific work struct heal monit APWSHM 2018; 2018. p. 410–8.
[25] Gulgec NS, Takáč M, Pakzad SN. Convolutional neural network approach for robust structural damage detection and localization. J Comput Civ Eng 2019;33(3):04019005. https://doi.org/10.1061/(ASCE)CP.1943-5487.0000820.

[26] A. Kundu, M. Price, D. Riordan, Theory and practice of aircraft performance, 2016.
[27] Melin T. A vortex lattice MATLAB implementation for linear aerodynamic wing applications. R Inst Technol Sweden; 2000.
[28] Rozylo P. Failure analysis of thin-walled composite structures using independent advanced damage models. Compos Struct 2021;262:113598. https://doi.org/10.1016/j.compstruct.2021.113598.
[29] Zhang H, Zhang L, Liu Z, Qi S, Zhu Y, Zhu P. Numerical analysis of hybrid (bonded/bolted) FRP composite joints: a review. Compos Struct 2021;262:113606. https://doi.org/10.1016/j.compstruct.2021.113606.
[30] Liu H, Liu J, Ding Y, Hall ZE, Kong X, Zhou J, et al. A three-dimensional elastic-plastic damage model for predicting the impact behaviour of fibre-reinforced polymer-matrix composites. Compos Part B Eng 2020;201:108389.
[31] Yan S, Zeng X, Long A. Experimental assessment of the mechanical behaviour of 3D woven composite T-joints. Compos Part B Eng 2018;154:108–13. https://doi.org/10.1016/j.compositesb.2018.08.007.
[32] LeCun Y, Bengio Y, Hinton G. Deep learning. Nature 2015;521(7553):436–44. https://doi.org/10.1038/nature14539.
[33] Deng L, Hinton G, Kingsbury B. New types of deep neural network learning for speech recognition and related applications: an overview. IEEE Int Conf Acoust Speech Signal Process 2013;2013:8599–603. https://doi.org/10.1109/ICASSP.2013.6639344.
[34] Alzubi J, Nayyar A, Kumar A. Machine learning from theory to algorithms: an overview. J Phys Conf Ser 2018;1142:012012. https://doi.org/10.1088/1742-6596/1142/1/012012.
[35] Ioffe S, Szegedy C. Batch normalization: accelerating deep network training by reducing internal covariate shift, in: 32nd int conf mach learn ICML 2015, vol. 1; 2015. p. 448–56.
[36] Li L, Jamieson K, Rostamizadeh A, Talwalkar A. Hyperband: a novel bandit-based approach to hyperparameter optimization. J Mach Learn Res 2018;18:1–52.



https://dspace.org/

Structure health monitoring of a composite wing based on flight load and strain data using deep learning method

Lin, Minxiao; Guo, Shijun; He, Shun; Li, Wenhao; Yang, Daqing

2022-01-29
Elsevier
https://doi.org/10.1016/j.compstruct.2022.115305
Lin M, Guo S, He S, et al., (2022) Structure health monitoring of a composite wing based on flight load and strain data using deep learning method. Composite Structures, Volume 286, April 2022, Article number 115305

Downloaded from a DSpace repository. https://dspace.org/